Available online at www.sciencedirect.com
SCIENCE DIRECT®
Journal of Magnetic Resonance 176 (2005) 64–70
JMR Journal of Magnetic Resonance
www.elsevier.com/locate/jmr

Profiles with microscopic resolution by single-sided NMR

J. Perlo, F. Casanova, B. Blümich *

Institut für Technische und Makromolekulare Chemie, RWTH, Aachen D-52056, Germany

Received 15 March 2005; revised 19 May 2005
Available online 21 June 2005

Abstract

A single-sided NMR sensor to produce depth profiles with microscopic spatial resolution is presented. It uses a novel permanent magnet geometry that generates a highly flat sensitive volume parallel to the scanner surface. By repositioning the sensitive slice across the object one-dimensional profiles of the sample structure can be produced with a space resolution better than 5 μm. The open geometry of the sensor results in a powerful testing tool to characterize arbitrarily sized objects in a non-destructive way.
© 2005 Elsevier Inc. All rights reserved.

Keywords: MRI; Single-sided NMR; Mobile probes; Microscopic resolution profiling; NMR-MOUSE

1. Introduction

Single-sided NMR sensors offer access to study arbitrarily sized objects non-invasively. They combine open magnets and surface RF coils to generate a sensitive volume external to the sensor and inside the object under investigation [1–5]. The price paid to gain in access is the impossibility of generating homogeneous magnetic fields. Nevertheless, this natural gradient can be exploited to obtain depth resolution into the material. The procedure is fully equivalent to the one used by the STRAFI technique [6], where the strong stray field gradient of superconducting magnets is used to measure profiles with high spatial resolution (in such a set-up, the superconducting magnets are used as large single-sided sensors). Although the strength of the static gradient generated by single-sided magnets is comparable to that in STRAFI experiments, the lateral gradients from small magnets results in rather poor depth resolution. Several attempts have been made to increase the gradient uniformity by tailoring the magnet geometry, but spatial resolution better than half a millimeter is hard to achieve [7–10]. Complicated magnet arrays have been the result of optimization procedures where the field profile is improved by playing with the position and orientation of a large number of permanent block magnets [9,10]. The philosophy adopted in previous designs requested the magnet to generate planes of constant field strength in large depth ranges. Such a profile is convenient because it allows selecting slices at different depths into the object simply by electronically switching the tuning frequency. Although the retuning procedure is simple and fast, we have detected deficiencies in this approach. Density profiles are contrasted by relaxation times or self-diffusion to improve the discrimination of heterogeneities in the material, but when the depth is changed the values of these parameters vary, introducing systematic changes in the contrast. For example, considering that the static field has a gradient of some T/m the resonance frequency changes by several MHz in a few millimeters. This poses a restriction to the use of T_1 contrast in samples with frequency dependent T_1. Moreover, the transverse relaxation time ($T_{2\text{eff}}$) measured by a CPMG sequence in inhomogeneous fields, which is a mixture of T_1 and T_2 [11], changes with the depth due to the variation of the B_0 and B_1 field profiles. Even the contrast by

* Corresponding author. Fax: +49 241 8022185.
E-mail address: bluemich@mc.rwth-aachen.de (B. Blümich).

1090-7807/$ - see front matter © 2005 Elsevier Inc. All rights reserved.
doi:10.1016/j.jmr.2005.05.017

diffusion is distorted as a consequence of the variation of the static gradient as a function of the depth.

During the last year, we have changed the scanning strategy going back to the original one used by the STRAFI technique, where the sample profiling is performed just by changing the relative position of the sample with respect to the sensitive slice keeping the excitation frequency constant [6]. Besides being a distortion free procedure, it only requires the generation of a flat sensitive slice at a single depth. This important reduction in constraints to the optimization procedure is exploited to produce higher depth resolution.

In this work, a single-sided NMR sensor intended for high resolution sample profiling is described. With it, microscopic depth resolution is achieved in situ for the first time with an open NMR sensor. By repositioning the sensor with respect to the sample, 1D profiles with a spatial resolution better than 5 μm are obtained. An important fact is that the magnet is of extremely simple construction and inexpensive to manufacture, which is important factor when such a tools are intended for quality control.

2. Sensor design

Magnets optimized to generate a uniform gradient in a large depth range are mainly based on the U-shape geometry, which uses two block magnets with antiparallel polarization placed on an iron yoke [3]. The important advantage of this magnet geometry relies on the fact that the static field is parallel to its surface, allowing its combination with simple and efficient surface RF coils. Recently, sensors based on simpler magnets like single solid bars or hollow cylinders [12,13] have been employed to generate near their pole faces a much more uniform magnetic gradient. But as the magnetic field generated by these geometries points along the depth direction, special planar RF coils are required to provide a B_1 field parallel to the magnet surface. Coil geometries, like figure-8 [12], are generally used in combination with these magnets, but they have two main disadvantages. First, the strong gradient of the B_1 field makes these coils inefficient for measurements at large depths. Second, they offer poor lateral selection, which is a critical issue when high depth resolution is required. The lateral dimensions of the plane where the magnets generate a constant magnetic field are finite and the selective excitation of this region is primarily determined by the design of the RF coil. On account of these facts, we decided for a magnet geometry with the static field parallel to the surface.

2.1. Magnet system

The poor depth resolution characteristic of the U-shaped geometry (Fig. 1 with $d_S = 0$) is fully determined by the lateral variation of the static field. Fig. 2 shows the spatial dependence of the magnetic field magnitude at different depths along the x and z directions. Although the field depends on the spatial coordinates in a complicated way, it can be approximated well by

$$|B_0(r)| = B_0(y) + \alpha(y)z^2 + \beta(y)x^2, \quad (1)$$

where $B_0(y)$ takes into account the main spatial variation along the depth, and α and β account for the lateral deviations at each depth. Since α and β have opposite signs, a sensitive volume with the shape of a horse saddle is defined. Although at the surface $|\alpha| > |\beta|$, the relationship is inverted $|\beta| > |\alpha|$ for large enough depth of the order of the magnet gap d_B.Therefore, for increasing depths, the sensitive volume becomes rather flat along z, and it is the curvature along x which determines the resolution.

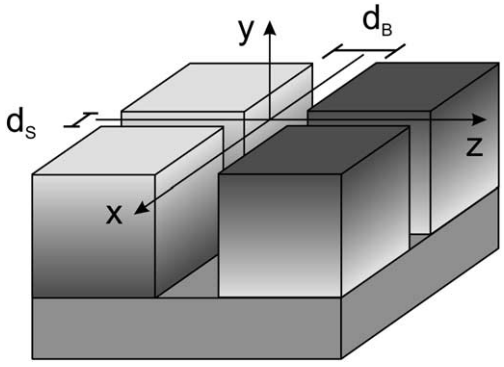

Fig. 1. The new magnet geometry used to generate a highly flat sensitive volume. It consists of four permanent magnet blocks positioned on an iron yoke. The direction of polarization of the magnets is indicated by the gray scale. Two magnets are polarized along y and two along $-y$. Magnets with the same polarization are separated by a small gap d_S (2 mm) while magnets with opposite polarization are separated by a gap d_B (14 mm). At 10 mm depth, the magnetic field points along z and has a magnitude of about 0.4 T, while the gradient is about 20 T/m and points along y.

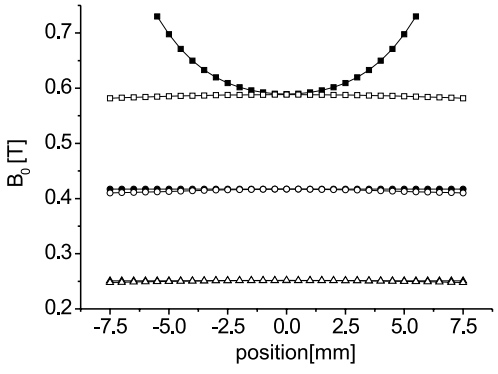

Fig. 2. Magnitude of the magnetic field along z (filled points) and x (empty points) at $y = 0$ (squares), 10 (circles), and 20 mm (triangles). The field magnitude was computed from the three field components scanned with a hall probe. It can be observed that the value of both $|\alpha|$ and $|\beta|$ in Eq. (1) becomes smaller with the increasing depth. They keep their sign, but α clearly goes to zero much faster than β.

To reduce $|\beta|$, the size of the magnet along x can be increased, but this brute-force solution leads to very large and heavy magnets. The solution presented in this work introduces a second gap d_S along x as shown in Fig. 1. To illustrate that, a set of B_0 profiles were measured for increasing d_S at $y = 10$ mm, and $z = 0$ (Fig. 3). For $d_S = 0$ (conventional U-shaped design), a strong variation of the field can be observed, while for a $d_S = 2$ mm the magnitude of the filed is almost constant in a region of 20 mm. If the gap is further increased to 4 mm the profile has the opposite curvature, showing that there is an optimum d_S for a constant field along x.

For a fine tuning of d_S, the magnetic field was scanned via the NMR resonance frequency of an oil film 10 μm thick and 2 mm wide confined between two glass plates. The high precision to measure the magnetic field strength in this way allows one to search for the final magnet positions to define the highest field uniformity.

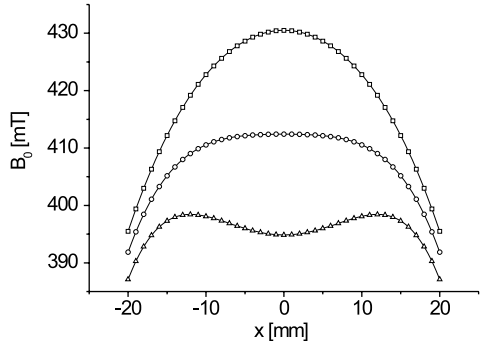

Fig. 3. Magnitude of the magnetic field along x for $d_S = 0$ mm (□), 2 mm (○), and 4 mm (△), at 10 mm from the magnet surface, and for $z = 0$. The field magnitude was computed from the three field components scanned with a hall probe, and fitted by a fourth order polynomial. The field profiles clearly show the change in the field curvature generated by the gap d_S along x.

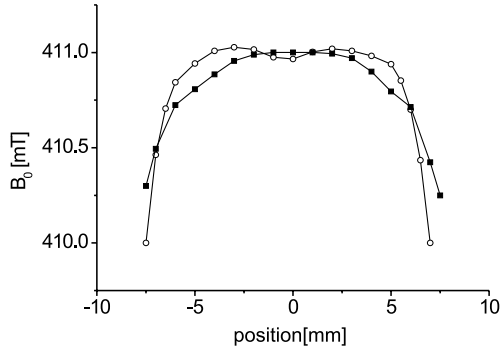

Fig. 4. Magnetic field magnitude measured at $y = 10$ mm via the resonance frequency of an oil film 10 μm thick and 2 mm wide. The field was scanned along x (solid points) and z (empty points) repositioning the film each millimeter and having the long side of the sample perpendicular to the scanned axis. The field variation in a region of 10 mm along both directions is smaller than 0.2 mT, which corresponds to a depth deviation smaller than 10 μm.

The field profiles shown in Fig. 4 have a variation smaller than 0.2 mT in a range of 10 mm along both x and z directions. Taking into account the magnitude of the static gradient, the field curvature can be converted to position to determine the depth variation, which results in less than 10 μm deviations from the planar geometry even at the corners of the scanned region.

It is important to point out, that the region where the field can be considered constant is limited. Beyond the limits, the lateral gradients increase dramatically. In general, the objects to be scanned are larger than the spot where the field is constant. Consequently, the lateral limitation of the sensitive volume is critical in the design of the RF coil of a sensor intended for high depth resolution.

2.2. Radiofrequency coil

The design of the RF coil to be used for sample profiling in combination with the present magnet has to account for two important issues. First, the coil dimensions must be set to select a 10×10 mm^2 spot in the x–z plane where the magnet defines a highly constant magnetic field. Second, the coil inductance must be kept to a minimum to reduce possible detuning due to loading changes introduced during the scanning procedure.

The RF coil designed to fulfill these requirements is a two-turn rectangular coil from 1.0 mm diameter copper wire. It is 14 mm long along x and 16 mm along z. The coil can be positioned at different distances from the flat slice to change the maximum penetration depth into the sample. When placed at 4 mm from the slice, the magnitude of the RF field is the half of the value at the surface.

A conventional tank-circuit is used for tuning and matching of the RF coil. The low coil inductance of about 0.06 μH requires 1400 pF to tune it to 17.5 MHz. The nominal quality factor (Q) of the circuit is 65, which leads to a dead time of about 20 μs. By introducing a resistance in parallel to the coil, the Q can be reduced to shorten the dead time. For example, with a resistance of 5 kΩ, a Q of 23 and a dead time of about 7 μs can be obtained. To test the change in the tuning and matching conditions, different samples like polymers, water and oil, biological samples, and rocks were place on top of the RF coil, obtaining a maximum shift in the resonance frequency of 9 kHz, 30 times smaller than the circuit bandwidth, and a negligible change from −40 to −37 dB in the reflected power.

2.3. Lift

The profiling method requires repositioning of the sensitive slice through the object. Hence, either the sample is moved with respect to the sensor or the sensor with respect to the sample. In practice, the second option appeared to be more convenient to us. Fig. 5 shows a

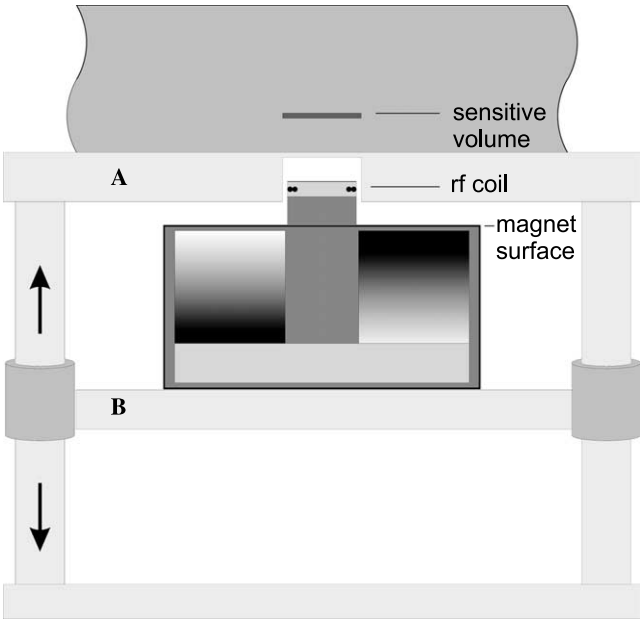

Fig. 5. Schematic of the *lift* used to reposition the sensitive slice across the sample with a precision of 10 μm. The object is placed on top of the plate A, which is parallel to the movable plate B where the sensor is mounted. In this way, the surface of the object can be precisely aligned with the flat sensitive slice. The drawing also illustrates the positions of the sensitive slice, the RF coil that defines the sensor surface, and the magnet surface.

schematic of the *lift* system used to reposition the sensor placed underneath the sample. The object under study is positioned on top of a flat holder (A) and the NMR sensor is placed on a movable plate (B). This mechanism allows one to move the sensor up and down with a precision of 10 μm.

3. Experiments and results

3.1. Spatial resolution

The spatial resolution achieved with a single-sided sensor is determined by the full-width at half-maximum (FWHM) of the point-spread function (PSF) like in any NMR imaging experiment. In the presence of an ideal gradient, this function can be calculated in terms of the maximum gradient strength, the line-width, etc. Nevertheless, in the present case the resolution limit is imposed by imperfections of the gradient, so that the PSF must be determined experimentally. It can be done by imaging a very thin object or as the derivative of the image of a step sample. Taking the second option, an oil film $5 \times 5\ \mathrm{cm}^2$ placed on a glass slide was imaged centering the oil–glass interface with the sensitive volume. The RF pulse length was set to 5 μs to excite a slice much thicker than the expected point-spread function. Fig. 6 compares the PSF at the surface of a conventional U-shaped magnet with the one obtained with the new

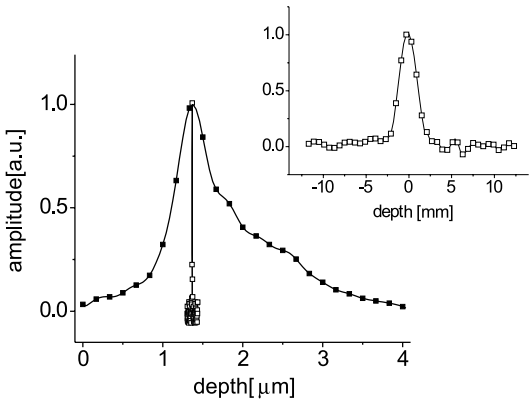

Fig. 6. Comparison of the PSF measured with the conventional U-shaped magnet (solid points) and the new 4-magnet design presented in this paper (empty points). The line for the U-shaped magnet was constructed by scanning the signal intensity of a sample layer 100 μm thick as a function of y. Its FWHM is about 1 mm, and it is not symmetric. The PSF for the 4-magnet geometry was obtained as the derivative of the step image of a glass–oil interface. The zoom demonstrates that the line-width is about 2.3 μm.

magnet geometry. To better appreciate the line-shape, a zoom is also displayed in this figure, showing that a FWHM of 2.3 μm is achieved.

It is worth noting that this high resolution was achieved using a sample with lateral dimensions much bigger than the spot where the static field can be considered constant. It confirms that the RF coil efficiently selects the limited region indicated in Fig. 4. From here on in this paper, the lateral dimensions of the samples are always much bigger than the dimensions of the RF coil. In experiments where a resolution poorer than 2.3 μm is used, the gradient can be considered uniform and the resolution calculated in terms of gradient strength and acquisition time.

The profiling procedure described in previous sections works by repositioning the sensor with respect to the sample and measuring a single-point per increment step. However, multiple points can be acquired by Fourier transformation of the echo signal if a thick enough slice can be properly excited [14]. The excitation bandwidth of the sequence can be calculated as the inverse of the length of the RF pulses used. If the RF power is large enough to apply short RF pulses, the quality factor of the RF circuit must be considered to determine the maximum bandwidth. As a consequence of the non-uniform excitation profile the image intensity suffer from important attenuation as a function of the frequency offset. In this work, we defined the maximum slice that can be imaged as the central region in the image of a uniform sample without appreciable intensity variation. For the present sensor configuration, it was determined to be 42 kHz, which corresponds to 50 μm. The Fourier imaging method can be combined with the stepwise procedure to reconstruct the profile in a straightfor-

ward fashion by plotting portions of 50 μm one next to the other. No correction, interpolation or smoothing is required at the places where two consecutive portions join. To illustrate the performance of the method, a phantom made up as a sandwich of two latex sheets 70 μm thick separated by a 150 μm glass slide was scanned (Fig. 7).

The high resolution can be appreciated from the sharp edges of each latex sheet. For this particular case, the RF coil was placed to define a maximum scanning range of 2 mm but it can be adjusted to the desired value by just changing the relative position between the coil and the magnet surface.

For some special applications where just a thin slice of no more than a few hundred microns needs to be imaged the Q factor can be reduced to completely excite the slice. When this is done no repositioning of the sample is required. It is worth pointing out that the only advantage of this approach is the elimination of the positioning device, but it does not lead to any time saving. When, for example, the Q is reduced a factor of 2 to double the slice thickness the measuring time to get the same S/N ratio is also doubled.

An interesting application of the method is the profiling of the multi-layer wall of a PE gasoline tank. Multilayer structures are widely used and can be found in almost any plastic packaging material. They often include thin barriers to reduce the permeation of specific compounds through the container wall. For the gasoline tank, a barrier layer is required to reduce the vapor emission below the legal limit, but these layers can also be made to act as oxygen barriers in food packages. The barrier is mainly made of an ethylene-vinyl-alcohol-copolymer (EVOH), which is glued to high density polyethylene (HDPE) by some resin. The present wall structure consists of five layers. From the outside to the inside they are regrind, resin, EVOH, resin, and HDPE (Fig. 8).

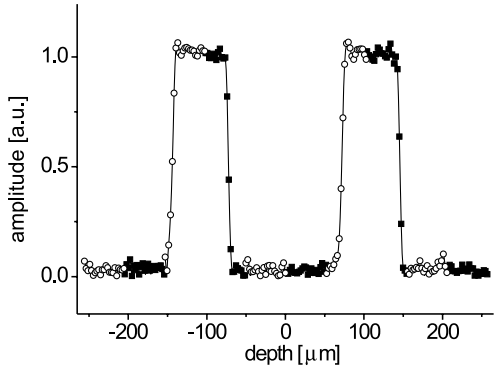

Fig. 7. One-dimensional profile of a sample made of two thin latex layers 70 μm thick separated by a glass spacer 150 μm thick. The full profile has a field of view of 500 μm. It is the combination of a set of images with a FoV of 50 μm acquired by repositioning the sensor in steps of 50 μm to cover the desired spatial range. Each of these images is the FT of the echo signal obtained as the addition of the first 16 echoes acquired with a CPMG sequence with an echo time $t_E = 345$ μs and 512 scans. Using a recycle delay of 50 ms, each image took 30 s and the total profile 5 min. In this experiment, the acquisition window was set to 300 μs, which in the presence of a gradient of 20 T/m defines a nominal resolution of 4 μm.

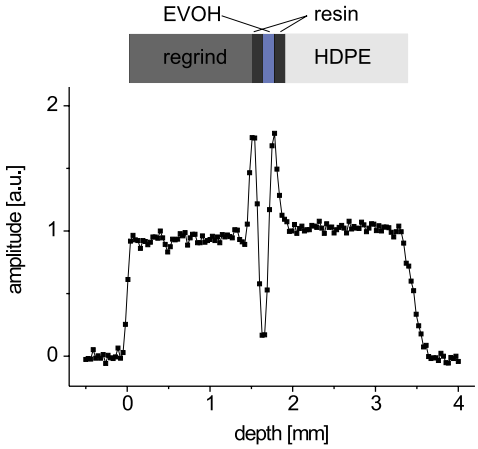

Fig. 8. One-dimensional profile of the wall of a PE gasoline tank. T_1 and T_2 were measured across the sample, and uniform values of about 90 ms and 300 μs were obtained. The profile intensity is the addition of the first eight echoes acquired with a solid-echo train with $t_E = 40$ and 4 μs long RF pulses. A nominal spatial resolution of 50 μm was defined by setting the acquisition window to 20 μs. The position of the sensor was moved in steps of 25 μm requiring 160 points to cover the complete sample thickness. Using 512 scans per point and a recycle delay of 150 ms, a total time of 75 s was required for each point.

This material possesses a short T_{2eff} of the order of 300 μs and can be taken as realistic test case to appreciate the sensitivity and resolution of the sensor. The amplitude of each point in the profile is the addition of the first eight echoes acquired by applying a solid-echo train with $t_E = 40$ and 4 μs long RF pulses. Notice that the depth selection is not achieved by applying selective RF excitation. Actually, the RF pulses are always set to guaranty a uniform excitation across the slice and to keep relaxation during the pulses to a minimum, while the depth resolution is achieved by controlling the length of the acquisition window. In general, when the desired spatial resolution is comparable to the maximum excitation bandwidth, just the point at zero frequency is taken from the FT of the echo signal.

3.2. Relaxation and diffusion contrast

The slice selection procedure can be combined with a number of pulse sequences to spatially resolve NMR parameters or to contrast the profiles with a variety of filters. The one most commonly used is the CPMG sequence, which is implemented to measure the transverse relaxation time. In this case, the complete echo train decay can be acquired and fitted to determine the T_{2eff} or

different parts of the train can be co-added to obtain relaxation time weighted profiles. We have found this last option more convenient, especially when the decay has a complicated time dependence, or when $T_{2\mathrm{eff}}$ or at least one component of the decay is comparable with the echo time t_E. Therefore a weighting function is defined as follows:

$$w(i_i, i_f, j_i, j_f, t_E) = \frac{i_i - i_f}{j_i - j_f} \sum_{j=j_i}^{j_f} S(jt_E) / \sum_{i=i_i}^{i_f} S(it_E), \qquad (2)$$

where $S(t)$ is the intensity of the signal at time t. The integration limits i_i, i_f, j_i, and j_f are adjusted to obtain the optimum contrast. To illustrate the performance of this method, a sample made of three natural rubber sheets with different cross-link densities separated by glass slides 150 μm thick was imaged (Fig. 9).

Since the first works on single-sided sensors it was suggested that the natural static gradient could be used to measure the self-diffusion coefficient of liquid-like samples. Nevertheless, the poor gradient uniformity always limited the accuracy of this type of experiment. Some approaches used the real spatial variation of the gradient magnitude to deconvolute the distribution of decays across the sensitive volume using post-processing, but this method is very time consuming and offers poor accuracy [15]. The magnet geometry presented here generates a magnetic field with a quite uniform gradient, so that straightforward methods like the Hahn or stimulated echo sequences can be used. Different liquids have been measured by incrementing the t_E of the Hahn echo sequence. Following the Hahn-echo filter, a CPMG sequence was applied to generate an echo train

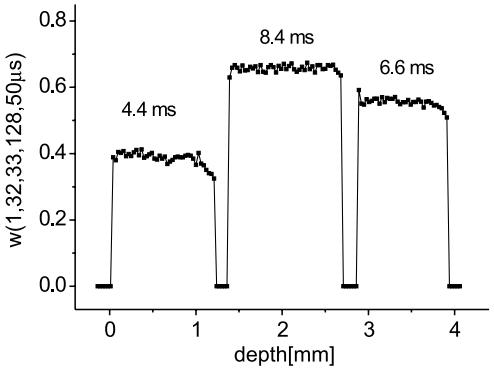

Fig. 9. One-dimensional profile of a phantom made of three rubber layers with different cross-link densities separated by glass spacers 150 μm thick. The profile amplitude corresponds to the weighting function w calculated with $i_i = 1$, $i_f = 32$, $j_i = 33$, and $j_f = 128$ (in Eq. (2)). The method allows a fast discrimination of the cross-link densities. The $T_{2\mathrm{eff}}$ obtained from the data fitting are displayed in the plot. It is observed that the values of the weighting function correlate with $T_{2\mathrm{eff}}$. In regions where the signal was close to zero the weighting function was not evaluated and a zero value was assigned to the profile.

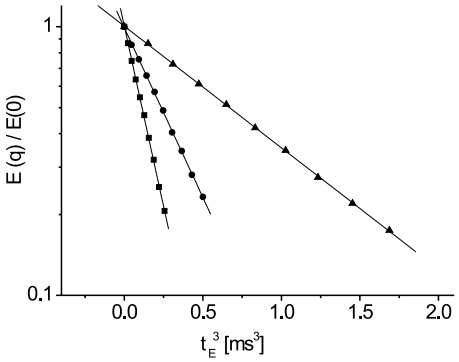

Fig. 10. Attenuation of the signal amplitude as a function of the echo time t_E of the Hahn-echo sequence. Although the gradient strength was first estimated to be 20.0 T/m by imaging methods, it was recalculated with higher precision by the water diffusion experiment (■) to 20.65 T/m. From the slopes of the linear fits, the diffusion coefficients of ethanol (●) and hexadecane (▲) were calculated as 0.974×10^{-9} and 0.349×10^{-9} m^2/s, respectively, which are in very good agreement with the values reported in literature [16,17]. All measurements were performed at 22 °C. For sensitivity improvement, a CPMG sequence was applied after the formation of the Hahn-echo. In these experiments, 1000 CPMG echoes were co-added, reducing the experimental time to measure each diffusion curve to less than a minute.

for detection with improved sensitivity. Fig. 10 shows the experimental data for water, ethanol, and hexadecane, together with linear fits. The uniformity of the gradient can be evaluated from the very good agreement between the signal decay and the correspondent linear function. Thanks to the sensitivity improvement obtained by the addition of the echo train, a measuring time shorter than 1 min was required for each diffusion curve.

3.3. Scanning large depths

In many cases, not only high spatial resolution but also a large penetration depth is desired. It can be achieve by increasing the dimensions of the magnet blocks and gaps keeping their proportion fixed. When the magnet is scaled up the depth where the plane of constant field is generated as well as the maximum resolution are scaled up by the same factor. Although the magnet scaling is the natural procedure to reach larger depths, it leads to a non-desired increase in the sensor size. A more elegant solution is to keep the sizes of the magnet blocks constant and to increase the gaps keeping their proportions fixed. A second prototype generating a flat slice at 18 mm from the magnet surface was built using $d_B = 20$ mm and $d_S = 3$ mm. At this depth, the magnetic field is $B_0 = 0.25$ T and the static gradient is $G_0 = 11.1$ T/m. Combining this magnet with an RF coil 22×25 mm^2, a working depth of 10 mm was defined. An object made of three rubber layers separated by glass spacers with a total thickness of 10 mm was scanned, and the results are shown in Fig. 11. It is important to

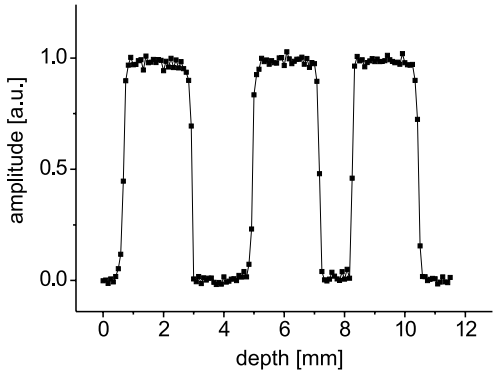

Fig. 11. Profile of a phantom made of three rubber layers 2 mm thick separated by glass slides 2 and 1 mm thick. The CPMG sequence was executed with the following parameters: repetition rate, 50 ms; t_E, 0.12 ms; number of echoes, 48 and 64 accumulations. The profile was scanned in 5 min with a spatial resolution of 100 μm.

stress the very good sensitivity of the device. Each point in the profile corresponds to a 100 μm thick slice at 10 mm from the sensor requiring a measuring time of only 3 s.

4. Conclusions

A single-sided NMR sensor that provides a depth resolution better than 5 μm was presented. It takes advantage of a new and simple magnet geometry that generates a magnetic field with an extremely uniform gradient to resolve the near surface structure of arbitrarily large samples. The scanning procedure requires repositioning the sensor. It keeps the measurement conditions constant and eliminate systematic errors introduced otherwise in the relaxation times and diffusion weight. The sensor was equipped with a low inductance RF coil which is insensitive to loading changes during the scanning procedure avoiding the necessity of retuning. The definition of a flat sensitive volume is advantageous not only from the imaging point of view: single-sided sensors are also used to study thin samples like paper sheets and old documents, where an important sensitivity improvement is expected from the larger intersection of the sample and the sensitive volume. Furthermore, background signals from the sensor housing are completely eliminated. Potential use of the profiling technique is envisioned in a large number of applications like the measurement of moisture profiles, the effects of cosmetics in human skin, solvent ingression in polymers, and the state assessment of paintings and other objects in efforts to conserve cultural heritage.

Acknowledgments

Special thanks to K. Kupferschläger for the design and construction of the mechanical lift used to reposition the sensor with high precision. Support of this project by the DFG Forschergruppe FOR333 Surface NMR of Elastomers and Biological Tissue is gratefully acknowledged.

References

[1] J.A. Jackson, L.J. Burnett, F. Harmon, Remote (inside–out) NMR. III. Detection of nuclear magnetic resonance in a remotely produced region of homogeneous magnetic field, J. Magn. Reson. 41 (1980) 411–421.
[2] R.L. Kleinberg, A. Sezginer, D.D. Griffin, M. Fukuhara, Novel NMR apparatus for investigating an external sample, J. Magn. Reson. 97 (1992) 466–485.
[3] G. Eidmann, R. Salvelsberg, P. Blümler, B. Blümich, The NMR-MOUSE, a mobile universal surface explorer, J. Magn. Reson. A122 (1996) 104–109.
[4] R.L. Kleinberg, Well logging, in: D.M. Grant, R.K. Harris (Eds.), Encyclopedia of NMR, Wiley, New York, 1996, pp. 4960–4969.
[5] G.A. Matzkanin, A review of non-destructive characterization of composites using NMR, in: Nondestructive Characterization of Materials, Springer, Berlin, 1998, p. 655.
[6] P.J. McDonald, Stray field magnetic resonance imaging, Prog. Nucl. Magn. Reson. Spectrosc. 30 (1997) 69–99.
[7] P.J. Prado, NMR hand-held moisture sensor, Magn. Reson. Imaging 19 (2001) 505–508.
[8] F. Casanova, B. Blümich, Two-dimensional imaging with a single-sided NMR probe, J. Magn. Reson. 163 (2003) 38–45.
[9] J. Perlo, F. Casanova, B. Blümich, 3D imaging with a single-sided sensor: an open tomograph, J. Magn. Reson. 166 (2004) 228–235.
[10] P.J. Prado, Single sided imaging sensor, Magn. Reson. Imaging 21 (2003) 397–400.
[11] M.D. Hürlimann, D.D. Griffin, Spin dynamics of Carr-Purcel-Meibohm-Gill-like sequences in grossly inhomogeneous B_0 and B_1 fields and applications to NMR well logging, J. Magn. Reson. 143 (2000) 120–135.
[12] B. Blümich, V. Anferov, S. Anferova, M. Klein, R. Fechete, M. Adams, F. Casanova, A simple NMR-MOUSE with a bar magnet, Magn. Reson. Eng. 15 (4) (2002) 255–261.
[13] S. Rahmatallah, Y. Li, H.C. Seton, I.S. Mackenzie, J.S. Gregory, R.M. Aspden, NMR detection and one-dimensional imaging using the inhomogeneous magnetic field of a portable single-sided magnet, J. Magn. Reson. 173 (2005) 23–28.
[14] P.J. McDonald, B. Newling, Stray field magnetic resonance imaging, Rep. Prog. Phys. 61 (1998) 1441–1493.
[15] M. Klein, R. Fechete, D.E. Demco, B. Blümich, Self-diffusion measurements by a constant-relaxation method in strongly inhomogeneous magnetic fields, J. Magn. Reson. 164 (2003) 310–320.
[16] Reported in the Bruker Almanac 2002.
[17] S. Vasenkoy, P. Galvosas, O. Geier, N. Nestle, F. Stallmach, J. Käerger, Determination of genuine diffusivities in heterogeneous media using stimulated echo pulsed filed gradient NMR, J. Magn. Reson. 149 (2001) 228–233.